Transition metal superlattices and epitaxial films on Ir(100)-(5×1)-H

C. Giovanardi, A. Klein, A. Schmidt, L. Hammer, and K. Heinz
Lehrstuhl für Festkörperphysik, Universität Erlangen-Nürnberg, Staudtstrasse 7, D-91058 Erlangen, Germany
(Received 21 July 2008; revised manuscript received 17 October 2008; published 12 November 2008)

The nanostructured phase Ir(100)-(5×1)-H is used as a template for the self-organized formation of nanometer-scaled lateral superlattices of the transition metals (TMs) Fe, Co, and Ni. Initially, Fe atoms decorate the monatomic Ir wires which reside in fivefold periodicity on the template. This is in contrast to Co and Ni which form islands within the adsorption stripes between and across the Ir wires. In no case there is intermixing with substrate atoms. At 0.8 monolayer coverage all stripe sites are filled so that lateral $\{TM_4Ir\}$ superlattices are formed. With further deposition a second TM layer grows, whereby the Ir wires at the interface remain immobile. Due to the different radii of atoms within the interface layer a substantial buckling is imprinted in the growing film as well as in the supporting substrate. The related morphology and crystallographic structure of the films are determined by atomically resolved scanning tunneling microscopy and quantitative low-energy electron diffraction.

DOI: 10.1103/PhysRevB.78.205416 PACS number(s): 61.46.Km, 61.05.jh, 68.55.−a

I. INTRODUCTION

Advances in storage and information technologies and the discovery of unusual magnetic behavior for materials with reduced dimensionality (for example, see Refs. 1–3) have urged to grow and characterize magnetic nanostructures as model systems for both fundamental studies and applications. Numerous attempts to tailor materials on the nanometer scale have shown that the fast and reproducible production of long-range ordered and defect-poor nanostructures is not an easy task. The "bottom-up" procedure appears to be favorable compared to the "top-down" approach as it profits from the self-assembly of material on a suitable substrate which, however, is not always available with the desired properties. Concerning the preparation of linear nanostructures—which is the issue of this paper—it has been demonstrated that, for instance, although Co chains can be produced by decoration of step edges on a platinum surface, this procedure does not apply for Ni, which intermixes with the substrate.[4] Kinks and defects in the step edges of metal surfaces affect the order and length of the chains. Semiconductor surfaces, instead, often exhibit almost defect-free steps, which can be decorated by several metals.[5] However, with magnetic transition metals (TMs) alloying occurs. Preferential channels for one-dimensional diffusion, and therefore, good candidates for chain growth are the troughs of missing row reconstructed surfaces.[6] However, the lateral spacing between these easy diffusion channels is rather small, and so a strong lateral interaction between the adsorbate chains is expected. Also other surface reconstructions proved to be proper templates to grow metallic chains but either the surface inhomogeneity or the release of the reconstruction itself limited the formation of chain phases all over the full sample surface.[7,8]

In our study, we use a special phase of the Ir(100) surface as template, which is its hydrogen-stabilized Ir(100)-(5×1)-H phase. It results from the well-known quasi-hexagonal reconstruction of the clean surface, Ir(100)-(5×1)-hex,[9,10] by restructuring upon H_2 adsorption.[11] The (5×1)-H phase is a real nanostructured template with micrometer-long and defect-free monatomic iridium wires residing on the (1×1) bulk-terminated substrate (Fig. 1). They are arranged in parallel in ⟨011⟩ directions with (5×1) periodicity (i.e., spaced by $5a_p^{\mathrm{Ir}}$ with $a_p^{\mathrm{Ir}}=2.715$ Å as iridium's in-plane lattice parameter). Yet, as visualized by the scanning tunneling microscopy (STM) image in Fig. 1(a) this periodicity and spacing are only on average, i.e., there are—in addition to the dominant spacing $5a_p$—also occasional spacings $3a_p$ and $7a_p$. The latter alternates with the other[11] so that the long-range (5×1) periodicity is not disturbed. Equivalently, the low-energy electron diffraction (LEED) pattern is of (5×1) symmetry as apparent from the electron-diffraction pattern in Fig.

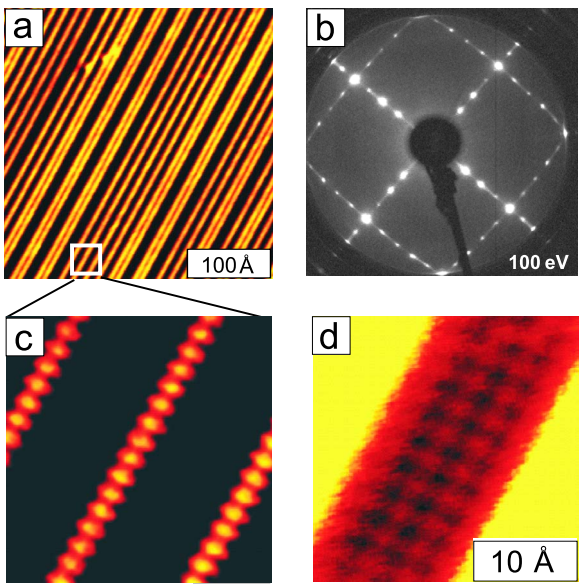

FIG. 1. (Color online) STM images and LEED pattern of the Ir(100)-(5×1)-H surface at different scales. Panel (a) displays the arrangement of Ir wires in (on average) fivefold periodicity, panel (c) shows the wires with atomic resolution, and in panel (d) next layer atoms in the space between the wires are shown to be in square arrangement. Panel (b) displays the LEED pattern of the (5×1) superstructure appearing in two orthogonal domains.

1(b) (note that there are two orthogonal domains due to the square symmetry of the substrate). The spaces between the Ir wires present unidirectional and separated adsorption stripes for deposition of material with a maximum coverage of 0.8 monolayer (ML) in this layer. As the spacing of the wires amounts to 1.36 nm (on average), nanostructures (in the real sense of the word) should develop. Indeed, deposition of Fe on Ir(100)-(5×1)-H has been found by our group to lead to such nanostructures, namely, laterally periodic {FeIrFe} sandwich chains at 0.4 ML coverage and a lateral $\{Fe_4Ir\}$ superlattice at 0.8 ML coverage.[12]

In the present paper we investigate and compare the growth of Fe, Co, and Ni on Ir(100)-(5×1)-H. We first show that growth of the first layer is substantially different for Fe on one hand and Co and Ni on the other hand (for Fe we recall results already published). Then the coverage regime for all three TMs is extended to the deposition of a second layer in order to investigate the role and stability of the chemically mixed and structurally corrugated interface. The investigations are made by means of STM and quantitative LEED, a combination by which both the morphology and the full crystallography of the different films can be determined. We describe the corresponding experimental and computational details in Sec. II. Then we present the film growth and morphology in Sec. III and the structural parameters retrieved from quantitative LEED in Sec. IV. All results are discussed and summarized in Sec. V.

II. EXPERIMENTAL AND COMPUTATIONAL DETAILS

The experiments were performed in ultrahigh vacuum (UHV) using a commercial STM of the "Johnny Walker" beetle design (RHK Technology, Inc.) operated at room temperature and a home-made retractable back view LEED optics as described in detail earlier.[12] Evaporators for Fe, Co, and Ni were operated by electron bombardment of high-purity rods, whereby the pressure was not raised by more than 2×10^{-11} mbar during deposition. The deposition rate (0.1–0.5 ML/min) was calibrated by means of a quartz microbalance and further checked by STM with an accuracy of about 0.05 ML for the eventual coverage. The sample temperature was measured by a directly attached NiCr-Ni thermocouple. Atomically resolved STM images were taken with a sample bias of a few millivolts while the others with typically about 0.5 eV. LEED intensity vs energy spectra, $I(E)$, were recorded using a computer controlled video-based method,[13] whereby the sample was kept at 90 K. The primary beam incidence was normal to the surface, and its energy was varied between 50 and 600 eV in steps of 0.5 eV. The full diffraction patterns at each step were recorded on a hard disk within a total time of measurement of not more than 15 min. The intensities of the different diffraction beams were then evaluated off line by a pixel-wise summation within a square framing the spot under consideration and subtraction of background intensities determined at the frame edge. Spectra of symmetrically equivalent beams were averaged in order to increase the signal-to-noise ratio.

The Ir(100) surface exhibits, after the usual preparation procedure,[10] the well-known quasihexagonal reconstruction, Ir(100)-(5×1)-hex,[9,10] which appears in two orthogonal domains. Upon hydrogen adsorption the hexagonally reconstructed phase restructures to form the above described Ir(100)-(5×1)-H phase again appearing in two orthogonal domains which extend to thousands of angstroms.[11] This (5×1)-H phase is stabilized by hydrogen atoms which reside exclusively in bridge sites both on the (100) nanoterraces between the Ir wires and on those wires themselves.[14] The latter most probably stays at their sites under deposition of TMs while hydrogen on the nanoterraces desorbs as found by separate thermal-desorption measurements for a slightly thicker Ni film (2.8 ML).

LEED intensity analyses for the different films were performed using the perturbation method tensor LEED (Refs. 15 and 16) with the TENSERLEED program package applied.[17] Due to the different scattering characteristics of Ir on one hand and Fe, Co, and Ni on the other hand, intermixing of Ir with the TM could be checked by chemical tensor LEED (Refs. 13, 18, and 19) applying the average t-matrix approximation (ATA).[20] By the same method vacancies within the films were treated. The structural search was made by a frustrated simulated annealing procedure[21] guided by the Pendry R factor[22] which was also used to quote the quality of the eventual best fit between experimental and model spectra. The variance of the R factor,[22] $\mathrm{var}(R)=R\sqrt{8V_{0i}/\Delta E}$, was used to estimate the statistical errors of the analyses with ΔE as the energy width of the total database accumulated over all beams and $V_{0i}=5$ eV as the optical potential describing electron attenuation. By this estimation, however, correlations between parameters are neglected so that the real error limits can be larger, whereby experience shows that this can be by a factor of two.

III. GROWTH AND MORPHOLOGY OF THE FILMS

A. Films up to one monolayer thickness

We first address the initial growth of Ni and Co films in the range of up to 0.4 ML coverage and compare it to that of Fe investigated earlier.[12] For the latter data are available for 0.4 ML coverage, and Fig. 2 compares the corresponding STM image for Fe with that for Ni for deposition at room temperature [panels (a) and (b), respectively]. As obvious, Ni grows in islands within the adsorption stripes while the Fe atoms are attached to the Ir wires forming long chains of {FeIrFe} linear sandwich structures. The island formation in case of Ni is even more evident for smaller coverage values [panel (c)] and develops also for Co [panel (d)]. Apparently, the Ni and Co islands are laterally correlated beyond the separating Ir wires so that, as a whole, they appear extended normal to the wires. For increased (reduced) deposition temperature (not shown) the extension of the islands in direction of the stripes is increased (reduced) due to the higher (lower) mobility within the unidirectional adsorption stripes. There were no hints for cross-channel diffusion.

With increasing Ni (or Co) deposition the space between the Ir wires is gradually filled, whereby the islands grow mainly in direction of the adsorption stripes. As a consequence of the islands lateral correlation uncovered areas are also laterally correlated as demonstrated in Fig. 3(a) for a Co

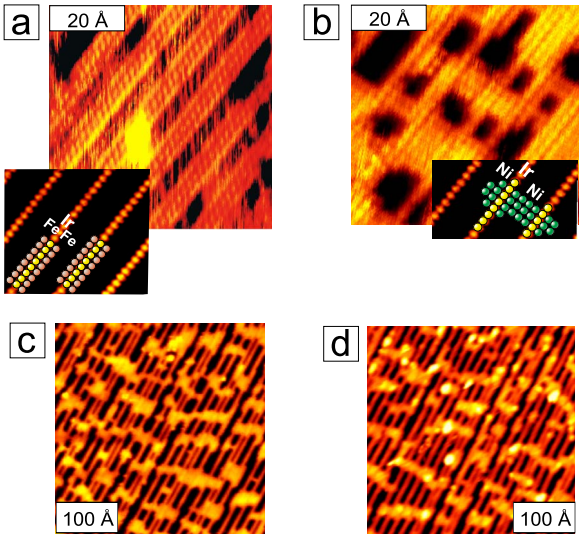

FIG. 2. (Color online) STM images for (a) 0.4 ML Fe, (b) 0.4 ML Ni, (c) 0.2 ML Ni, and (d) 0.2 ML Co. In panels (a) and (b) STM images of the uncovered surface are attached [similar to that in panel (c) of Fig. 1] with adatoms artificially inserted.

layer close to completion. Eventually, when the layer is completed (nominally at 0.8 ML coverage) the islands within the adsorption stripes coalesce and form—together with the Ir wires—a full monolayer equivalent to an ordered TM_4Ir surface alloy or a $\{TM_4Ir\}$ lateral superlattice. The narrow adsorption stripes ($3a_p^{Ir}$ width) are more quickly filled than broader stripes. This is because there are only two free adsorption sites equivalent to a linear density of only $\frac{2}{3}a_p^{Ir}$ while, e.g., on a stripe of $5a_p^{Ir}$ width the linear density of the four free sites is $\frac{4}{5}a_p^{Ir}$. At a coverage of nominally 0.8 ML [Fig. 3(c) for Ni] the layer completion is almost perfect, i.e., there only about 10% adatoms in the second adsorption layer

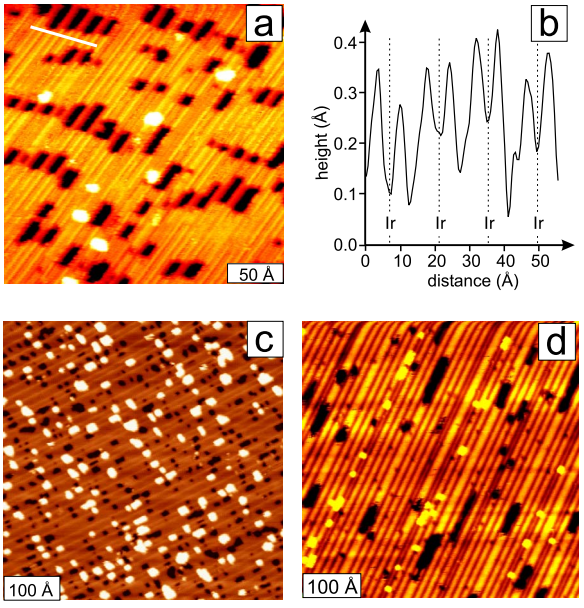

FIG. 3. (Color online) STM images for (a) ≈0.75 ML Co, (c) 0.8 ML Ni, and (d) 0.8 ML Fe for comparison. In panel (b) the profile along the line inserted in panel (a) is displayed.

and the same amount of holes in the first one [this holds also for deposition of Co and Fe whose STM image at 0.8 ML coverage is displayed in Fig. 3(d) for comparison].

All STM images displayed in Fig. 3 contain dark lines with (on average) a spacing of $5a_p^{Ir}$. It can be taken from atomically resolved images that these lines correspond to the Ir wires which separate neighbored adsorption stripes. Their position is not affected by the deposition of the TM. They appear to be pressed into the surface relative to the neighboring TM metal areas. This is by about 0.1–0.2 Å as visualized for Co quantitatively in Fig. 3(b) which displays the profile taken along the line inserted in panel (a). This feature holds for Ni and Co as well as for Fe although to an element specific extent. Additionally, in case of Co the atoms directly attached to the Ir wires appear to protrude considerably over those in the center of the adsorption stripe as can be seen in Fig. 3(b) (for Fe and Ni no significant height differences within the TM stripes can be detected).

It seems also to be possible to create a $\{TM_4Ir\}$ superlattice with TM species mixed in an ordered way. This should result by starting from the {FeIrFe} linear sandwich structure [Fig. 2(a)] and deposition of Co or Ni on that phase, filling the still empty sizes until layer completion. Yet, the resulting STM images are essentially the same as in Fig. 3(c), which is obviously due to the fact that the STM provides no chemical contrast to image Co or Ni different from Fe. As a consequence, we cannot safely prove that an ordered $\{FeTM_2FeIr\}$ superlattice is formed in this way but this is certainly a reasonable assumption.

B. Films of two monolayer thickness

By further deposition of Fe, Co, and Ni on the completed first monolayer, a second TM layer grows in each case again in pseudomorphic epitaxial arrangement. For higher coverage values stair-rod-like dislocations are formed which, however, are beyond the issue of the present paper and are presented separately.[23]

Figure 4 displays STM images and profiles for (as an example) Ni at a coverage of 1.8 ML, i.e., a film of 2 ML thickness including the Ir wires at the interface (the images for Fe and Co are rather similar). As apparent from the large-scale image there is again only a small percentage of holes in the second layer and a correspondingly small amount of islands already in the third one, i.e., there is almost ideal pseudomorphic layer-by-layer growth in the low coverage regime. The islands are much elongated in direction of the Ir wires. This is indicative for preferential one-dimensional diffusion due to the considerable buckling of the layers as apparent from the atomically resolved image [Fig. 4(b)]. The STM profile [Fig. 4(c)] reveals depression lines with depths in the range 0.2–0.3 Å and mutual spacings of 3 and $5a_p^{Ir}$ (there are also spacings with $7a_p^{Ir}$). The spacings show that the depressions mark the positions of interfacial Ir wires. In the spacings between the depression lines we count three, five, and seven local protrusions formed by Ni atoms. This indicates—just by sterical arguments—that the depression lines originate from troughs formed above the Ir wires within the underlying interface rather than from Ni rows imaged to

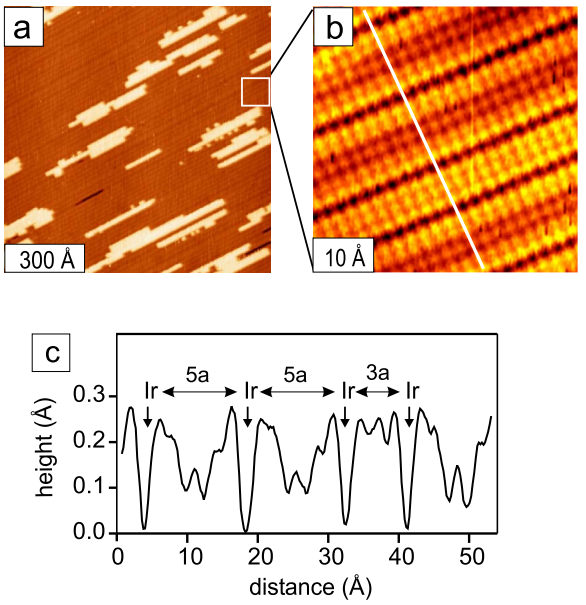

FIG. 4. (Color online) [(a) and (b)] STM images for 1.8 ML Ni. The height profile in panel (c) is along to the line inserted in (b) (the quantity a above the lateral arrows stands for $a_p^{\mathrm{Ir}}=2.715$ Å).

appear as dark lines as did the Ir wires within the first monolayer. It proves also that the interfacial $\{TM_4Ir\}$ superlattice survives under further TM deposition and creates a substantial corrugation in the growing film as observed in the STM images.

IV. QUANTITATIVE LEED STRUCTURE ANALYSES

The LEED intensities for all films were analyzed, assuming that the dominating spacing $5a_p^{\mathrm{Ir}}$ between the Ir wires is regular, although also spacings of $3a_p^{\mathrm{Ir}}$ and $7a_p^{\mathrm{Ir}}$ occur. Adatoms on the terminating layer were neglected. Due to the fact that the TMs deposited have rather close electron-scattering properties, we have not analyzed the mixed $\{FeTM_2FeIr\}$ phase for the 0.8 ML case. The structural parameters varied are defined in the model displayed in Fig. 5, whereby the layer counting starts with the third full Ir layer of the substrate (which turns out to be bulklike). Mirror symmetries according to the planes indicated by the broken lines were

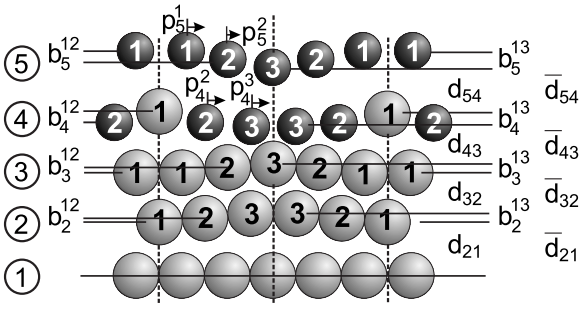

FIG. 5. Structural parameters for the different films (see text). Broken lines indicate applying mirror planes. Dark atoms correspond to TM atoms, shaded ones to Ir.

TABLE I. Structural results for the three $\{TM_4Ir\}$ phases (parameters are as defined in Fig. 5). The data for $\{Fe_4Ir\}$ are taken from Ref. 12.

	$\{Fe_4Ir\}$	$\{Co_4Ir\}$	$\{Ni_4Ir\}$
p_4^2(Å)	−0.05	0.00	0.01
p_4^3(Å)	0.03	−0.01	−0.02
b_4^{12}(Å)	0.10	0.11	0.11
b_4^{13}(Å)	0.11	0.14	0.14
c_4^2(%)	0	10	0
c_4^3(%)	10	30	10
d_{43}(Å)	1.67	1.76	1.71
$\bar{d}_{43}$(Å)	1.75	1.82	1.78
b_3^{12}(Å)	−0.09	−0.04	−0.02
b_3^{13}(Å)	−0.02	−0.05	−0.05
d_{32}(Å)	1.91	1.93	1.87
$\bar{d}_{32}$(Å)	1.96	1.96	1.91
b_2^{12}(Å)	−0.03	−0.01	0.00
b_2^{13}(Å)	−0.03	−0.02	−0.03
d_{21}(Å)	1.89	1.92	1.90
$\bar{d}_{21}$(Å)	1.91	1.93	1.91
ΔE (eV)	6400	6800	6300
R	0.11	0.18	0.15
var(R)	0.009	0.014	0.012

assumed to apply. The buckling amplitude $b_m^{ik}=z_m^i-z_m^k$ denotes the height difference of atoms i and k in the mth layer (with the coordinate z pointing out of the surface), p_m^i is the lateral shift of atom i in that layer (positive when toward the center mirror plane), and c_m^i is the vacancy concentration for those atoms. The quantity $d_{m,m+1}$ is the smallest spacing between layers m and $(m+1)$, and $\bar{d}_{m,m+1}$ is the spacing between the geometrical center planes of these layers. The qualitative arrangement of atoms in the model figure is already according to the scenario of the eventually determined structures (with little differences among Fe, Ni, and Co films), whereby, however, vertical distances and lateral atomic shifts off the ideal positions are exaggerated for better visibility.

For the 0.8 ML films the resulting best-fit parameters are displayed in Table I and compared to the case of $\{Fe_4Ir\}$ as taken from our earlier work.[12] For the 1.8 ML films the structural parameters are given in Table II. The tables contain also the best-fit R factors and their variance together with the total-energy width ΔE of the different databases. No intermixing of elements at the interface was found in agreement with the above-made assumption concerning the stability of the $\{TM_4Ir\}$ superlattice at the interface during film growth. The error limits as estimated by the variance of the R factor are typically about 0.02–0.03 and 0.03–0.05 Å for vertical parameters and parallel shifts, respectively (increasing slightly with layer depth), and about 10% for vacancy concentrations. As already mentioned these errors do not consider correlations between different parameters so that the real errors might be by a factor of two higher.

TABLE II. Results of the LEED analyses for TM films of nominally 1.8 ML coverage with the parameters as defined in Fig. 5.

	1.8 ML Fe	1.8 ML Co	1.8 ML Ni
p_5^1(Å)	0.16	0.17	0.16
p_5^2(Å)	0.03	0.01	0.00
b_5^{12}(Å)	0.13	0.10	0.07
b_5^{13}(Å)	0.19	0.15	0.12
c_5^1(%)	0	0	0
c_5^2(%)	20	20	10
c_5^3(%)	30	30	10
d_{54}(Å)	1.47	1.38	1.40
$\bar{d}_{54}$(Å)	1.71	1.59	1.61
p_4^2(Å)	−0.02	−0.03	0.01
p_4^3(Å)	−0.01	−0.03	−0.01
b_4^{12}(Å)	0.17	0.15	0.18
b_4^{13}(Å)	0.17	0.17	0.18
d_{43}(Å)	1.76	1.74	1.72
$\bar{d}_{43}$(Å)	1.80	1.80	1.78
b_3^{12}(Å)	−0.02	−0.01	0.01
b_3^{13}(Å)	−0.02	−0.03	−0.03
d_{32}(Å)	1.88	1.89	1.90
$\bar{d}_{32}$(Å)	1.91	1.91	1.91
b_2^{12}(Å)	−0.03	−0.01	0.00
b_2^{13}(Å)	−0.01	0.00	0.00
d_{21}(Å)	1.90	1.92	1.92
$\bar{d}_{21}$(Å)	1.92	1.92	1.92
ΔE (eV)	7500	6900	6400
R	0.20	0.19	0.12
var(R)	0.015	0.014	0.010

V. DISCUSSION AND CONCLUSION

As apparent from the STM images presented the Ir(100)-(5×1)-H surface is a very suitable template for the formation of linear nanostructures. Under deposition of the TMs Fe, Co, and Ni the regularly arranged and atomic-width Ir wires remain at their position. So the adatoms have the chance to decorate these Ir wires, analogous to the case of a stepped surface where they can decorate the atoms at the step edge—except that in the present case the decoration can take place at both sides of the wire. As resulting from quantitative LEED the adatoms do not exchange with the atoms of the Ir wires (or other template atoms) but—in the case of Fe but distinct from Co and Ni—just coordinate the wires from both their sides forming {FeIrFe} linear sandwich structures. This is different from the deposition of Fe on the stepped Cu(117) surface [exhibiting also fcc(100) terraces] for which first-principles calculations found that Fe is incorporated in the step below an inner corner site, in this way increasing its coordination.[24] Yet, there is a substantial activation energy involved in the corresponding exchange process. This might be even higher for Ir due to its stronger elemental bonding compared to Cu, and so it can be supposed that there is no exchange.[12] Also, the atomic radii of Fe, Co, and Ni (r_{Fe} = 1.24, r_{Co} = 1.25, and r_{Ni} = 1.24 Å) are rather different from that of Ir (r_{Ir} = 1.36 Å) such that substitution is assumed to be less favorable than for Fe in Cu (r_{Cu} = 1.28 Å).

On the other hand, Fe, Co, and Ni must be considerably strained [$\epsilon_{\|} = (r_{Ir} - r_{TM})/r_{TM} \approx 9\%$] both to decorate the Ir wires and to form pseudomorphic islands on the Ir(100)-(1×1) stripes between the wires which—as confirmed by the STM images and LEED analyses—takes place indeed. The tendency of Fe to form {TMIrTM} sandwich chains (which Co and Ni do not) is structurally mirrored by the fact that in the 1 ML film (0.8 ML TM deposited), the Fe atoms coordinating the Ir wires move toward the latter (p_4^3 = −0.05 Å, see Table I). which is in contrast to Co and Ni. This is in qualitative agreement with the formation enthalpies of the deposited TM with Ir which are provided in the literature by calculations applying semiempirical models.[25] The value for FeIr is with 9 kJ/mol (Ref. 26), which is much more favorable than for CoIr (3 kJ/mol) (Ref. 27) and NiIr (2 kJ/mol) (Ref. 28) such that Fe-Ir bonds are favored over Fe-Fe bonds leading to FeIrFe sandwich chains at 0.4 ML coverage. In contrast, the comparably small formation enthalpy for CoIr and NiIr leads to no preference of homogeneous or heterogeneous bonds, so there is island formation even beyond the Ir wires. Also, a weak cross-channel interaction may favor this formation as shown by kinetic Monte Carlo simulations for the system Ag/Ag(110) for which also thin adsorption channels separated by a monatomic Ag wire exist.[29]

In the STM images of the 1 ML films the Ir wires appear as dark lines, i.e., according to the profile [Fig. 3(b)] that is pressed into the surface by about 0.1–0.2 Å relative to the neighbored rows of TM metals. Yet, the LEED analyses retrieve that the Ir wires protrude from their TM neighbor rows by $b_4^{12} \approx 0.1$ Å. As a consequence, the STM feature must be due to electronic effects which overcompensate the geometrical buckling. Even more, only the TM rows coordinated by the Ir wires are resolved; the two-center TM rows in the (5×1) cell are unresolved and imaged much deeper (in particular in case of Co) as seen in the profile [Fig. 3(b)] although it is in all cases only $b_4^{13} - b_4^{12} \leq 0.03$ Å deeper in the surface. Obviously, the STM contrast strongly depends on the chemical environment of the rows imaged (and, of course, there is also some dependence on the bias voltage applied).

The chemically, and thus, also electronically inhomogeneous {TM_4Ir} interface layer also affects the structure of the template's pure Ir layers below. Atoms located below the Ir wires are significantly pressed into the surface compared to the height of those below the TM atoms [for the pure (5×1)-H phase the buckling is just reverse to that[11]]. A possible driving mechanism for that subsurface buckling might be that it allows for some reduction in the top layer corrugation. This surface smoothing is a common relaxation mechanism for geometrically rough (e.g., stepped) surfaces. Consistent with this argumentation deposition of another TM layer (1.8 ML films) is accompanied by an overall increase in the interface layer buckling while that in the Ir layer below is reduced. So, as found by quantitative LEED the b_4^{13} increases from 0.11–0.14 (for the different TMs) to 0.17–0.18 Å.

Equivalently, the second ML can be approximately understood as to reside carpetlike on the interface structure. The corresponding STM images are characterized by rather dark and narrow lines. As for the Ir wires on the uncovered (5×1)-H phase they have spacings of $3a_p^{\mathrm{Ir}}$, $5a_p^{\mathrm{Ir}}$, and $7a_p^{\mathrm{Ir}}$ (with $5a_p^{\mathrm{Ir}}$ being the average and dominating value) and are indeed located above the Ir wires at the interface. The dark line is due to the fact that each of the two atoms number one in the outermost layer exhibits a considerable lateral shift (p_5^1=0.16–0.17 Å), so a deep gap (of 0.32–0.34 Å width) is formed in which the STM tip can dive to a certain extent. Also, a broad and shallow trough of depth b_5^{13} =0.12–0.19 Å is formed in that layer by atoms {232} close to the value reproduced by the STM profile in Fig. 4(c) (it does not appear for lateral spacings of $3a_p^{\mathrm{Ir}}$).

Eventually we address the issue of the crystallographic type of our films as the native structure of Fe is of body-centered cubic (bcc) type while the Ir template is face-centered cubic (fcc). Certainly, for a 2 ML film a clear distinction between fcc and bcc from the crystallographic point of view is problematic. Fortunately yet, we can compare the present structural results with those we recently retrieved for Fe growth on the unreconstructed, i.e., flat Ir(100)-(1×1) surface with the pseudomorphic Fe layers unbuckled.[30] Interestingly, the first two Fe layers could be identified as a precursor structure to a face-centered tetragonally distorted (fct) structure, in particular, stress measurements showed that a corresponding film is under tensile strain rather than compressive strain, which is to be expected for a body-centered tetragonally distorted (bct) film. Surprisingly this fct precursor persists with further film growth although the further growing part of the film turns to bct structure. To resolve the structure type for our present case we cannot use interlayer spacings as the layers are considerably buckled due to the inhomogeneous interface layer. Yet, we can compare the bond lengths between Fe atoms in the two layers of the 1.8 ML film with those between nearest neighbors in bcc and fcc Fe which are—in view of the precision of our LEED analysis—sufficiently different, namely, 2.482 (bcc) and 2.527 Å (fcc). Evaluation of the LEED result shows that the bond lengths are in the range of 2.53–2.59 Å (average value of 2.565 Å). This includes the value of 2.53 Å found for the corresponding bond length in the 2 ML film on Ir(100)-(1×1),[30] clearly excluding bctlike bonding and favoring an fctlike film. Indeed, very recent stress measurements found consistently that—similar to Fe/Ir(100)-(1×1)—the strain is initially tensile also for Fe/Ir(100)-(5×1)-H.[31]

For the Ni and Co films of 1.8 ML coverage the structure type is fcc, which is similar to the substrate, as should be expected by the fact that Ni is fcc in its native structure and the hexagonal close packing (hcp) of Co is energetically nearly degenerate with its fcc structure. In fact for the Ni film the first to second layer bond lengths are in the range of 2.48–2.51 Å and for Co it is in the range of 2.49–2.52 Å which values are very close to those in the corresponding bulk fcc crystals (Ni: 2.492 Å, Co: 2.507 Å). In turn this demonstrates the accuracy and reliability of our LEED analysis.

In a last point we address the role of the hydrogen atoms which stabilize the Ir(100)-(5×1)-H phase. As already mentioned and found by first-principles calculations[14] the hydrogen atoms reside in this phase in bridge sites both of the Ir wires and on the terraces between the latter. Ni deposition causes the H atoms on the terraces to desorb while those on the Ir wires remain within the Ni film, most probably at or near their initial sites. Unfortunately, we have no information weather this also holds also for Co and Fe films. Yet, we have also performed experiments in which TMs were deposited on the hydrogen-free Ir(100)-(5×1)-hex phase. We found that the hexagonal reconstruction is lifted by the adatoms whereby—similar to the Ir(100)-(5×1)-H phase—Ir wires are also expelled to the surface. Yet, the long-range order is much worse. The LEED intensity spectra, however, are very similar for the two substrates both at 0.8 and 1.8 ML coverages proving that the local structures in the two cases are identical. This clearly indicates that the hydrogen atoms play no role in the development of the nanostructures described, except that the long-range order of the latter is much better when starting with the Ir(100)-(5×1)-H phase as template.

In conclusion we have shown that the Ir(100)-(5×1)-H surface is a suitable template to produce linear metallic nanostructures in a self-organized way. The regularly spaced Ir wires terminating this template provide adsorption channels so that upon Fe, Co, or Ni deposition lateral $\{TM_4Ir\}$ superlattices result when these channels are fully occupied. The Ir wires at the interface stay in their position of the (5×1)-H phase, and there is no intermixing of the TM atoms deposited with atoms of the Ir template. The different radii of Ir and the TM atoms lead to linearly corrugated TM films when the second TM layer grows. While on an ideally oriented Ir(100) surface all phases mentioned appear in two orthogonal domains: one of the latter can be suppressed using a stepped surface so that even fully unidirectional nanostructures can be prepared.

ACKNOWLEDGMENTS

The authors are indebted to Deutsche Forschungsgemeinschaft (DFG) for financial support. C.G. is grateful for stipends by the Alexander von Humboldt-Stiftung and by the European Commission through its Marie Curie Intra-European Programme.

[1] P. Gambardella, A. Dallmeyer, K. Maiti, M. C. Malagoli, and W. Eberhardt, Nature (London) **416**, 301 (2002).
[2] J. Shen and J. Kirschner, Surf. Sci. **500**, 300 (2002).
[3] S. D. Bader, Surf. Sci. **500**, 172 (2002).
[4] P. Gambardella, J. Phys.: Condens. Matter **15**, S2533 (2003).
[5] F. J. Himpsel, J. L. McChesney, J. N. Crain, A. Kirakosian, V. Peréz-Dieste, N. L. Abott, L. Yan-Yeung, and P. F. Nealey, J. Phys. Chem. B **108**, 14484 (2004).
[6] T. R. Linderoth, S. Horch, E. Laegsgaard, I. Stensgaard, and F. Besenbacher, Phys. Rev. Lett. **78**, 4978 (1997).
[7] L. Hammer, W. Meier, A. Schmidt, and K. Heinz, Phys. Rev. B **67**, 125422 (2003).
[8] G. Gurlu, O. A. O. Adam, H. J. W. Zandvliet, and B. Poelsema, Appl. Phys. Lett. **83**, 4610 (2003).
[9] A. Ignatiev, A. Jones, and T. Rhodin, Surf. Sci. **30**, 573 (1972).
[10] A. Schmidt, W. Meier, L. Hammer, and K. Heinz, J. Phys.: Condens. Matter **14**, 12353 (2002).
[11] L. Hammer, W. Meier, A. Klein, P. Landfried, A. Schmidt, and K. Heinz, Phys. Rev. Lett. **91**, 156101 (2003).
[12] A. Klein, A. Schmidt, L. Hammer, and K. Heinz, Europhys. Lett. **65**, 830 (2004).
[13] K. Heinz, Rep. Prog. Phys. **58**, 637 (1995).
[14] D. Lerch, O. Wieckhorst, L. Hammer, K. Heinz, and S. Müller, Phys. Rev. B **78**, 121405(R) (2008).
[15] P. J. Rous, J. B. Pendry, D. K. Saldin, K. Heinz, K. Müller, and N. Bickel, Phys. Rev. Lett. **57**, 2951 (1986).
[16] P. J. Rous and J. B. Pendry, Prog. Surf. Sci. **39**, 3 (1992).
[17] V. Blum and K. Heinz, Comput. Phys. Commun. **134**, 392 (2001).
[18] R. Döll, M. Kottcke, and K. Heinz, Phys. Rev. B **48**, 1973 (1993).
[19] K. Heinz, R. Döll, and M. Kottcke, Surf. Rev. Lett. **3**, 1651 (1996).
[20] Y. Gauthier, Y. Joly, R. Baudoing, and J. Rundgren, Phys. Rev. B **31**, 6216 (1985).
[21] M. Kottcke and K. Heinz, Surf. Sci. **376**, 352 (1997).
[22] J. B. Pendry, J. Phys. C **13**, 937 (1980).
[23] A. Klein, W. Meyer, A. Schmidt, B. Gumler, S. Müller, L. Hammer, and K. Heinz, Phys. Rev. B **78**, 045422 (2008).
[24] D. Spišák and J. Hafner, Phys. Rev. B **65**, 235405 (2002).
[25] A. K. Miedema, P. F. de Chatel, and F. R. de Boer, Physica B & C **100**, 1 (1980).
[26] R. Boom, F. R. de Boer, A. K. Niessen, and A. K. Miedema, Physica B & C **115**, 285 (1983).
[27] A. K. Niessen, A. K. Miedema, F. R. de Boer, and R. Boom, Physica B & C **151**, 401 (1988).
[28] A. K. Niessen, A. K. Miedema, F. R. de Boer, and R. Boom, Physica B **152**, 303 (1988).
[29] A. Videcoq, F. Hontifinde, and R. Ferrando, Surf. Sci. **515**, 575 (2002).
[30] V. Martin, W. Meyer, C. Giovanardi, L. Hammer, K. Heinz, Z. Tian, D. Sander, and J. Kirschner, Phys. Rev. B **76**, 205418 (2007).
[31] D. Sander (private communication).